CHEMICAL PREDICTIVE MODELING OF ACID MINE DRAINAGE FROM WASTE ROCK: MODEL DEVELOPMENT AND COMPARISON OF MODELED OUTPUT TO EXPERIMENTAL DATA[1]

William W. White III,[2] Edward M. Trujillo,[3] and Cheng-Kuo Lin[3]

Abstract: The U.S. Bureau of Mines (USBM) is developing a geochemical predictive model for acid mine drainage (AMD) from waste rock associated with metal mining. The model will identify AMD potential during property exploration and development and will facilitate planning of waste-rock handling. This paper presents results on model development and comparison of model output with 90 weeks of kinetic tests (humidity-cell data) for three selected samples. The existing model successfully matched experimental data collected from humidity-cell effluent during the 90-week period. The model (1) predicted the progressive development of acid as well as the decrease in aqueous sulfate and iron concentrations as jarosite precipitated and (2) demonstrated good agreement between modeled output and actual effluent pH, total iron, and sulfate concentrations from the three different samples of waste rock. Sulfide contents of these three samples were 3, 6, and 24 wt %. Although acid-base accounting classified all three samples as potential acid producers, effluent pH from the 3% pyrite sample was neutral to slightly basic during 90 weeks of accelerated weathering. Samples containing 6% and 24% pyrite continuously produced acidic effluent during the same 90-week period. Sulfate-release rates resulting from sulfide oxidation increased with solid-phase sulfide content and decreasing pH. Calcium and magnesium release-rates determined from accelerated weathering of the 3% pyrite sample were projected beyond 90 weeks. This projection suggests that the 3% pyrite sample should develop AMD after 110 to 130 weeks of laboratory-accelerated weathering. The mathematical model also predicts that AMD will occur after 130 weeks.

Additional Key Words: acid mine drainage, metal-mine waste rock, laboratory-accelerated weathering, geochemical predictive model.

Introduction

The purpose of the USBM's AMD predictive-modeling research is to (1) assist Federal land-managing agencies and industry with this assessment during the exploration and feasibility-study stages of a project and (2) apply the resulting model to the assessment of proposed AMD-treatment and -control scenarios. Model development is a cooperative effort between the USBM and the University of Utah Chemical and Fuels Engineering Department (University). Static and kinetic laboratory tests are being conducted by the USBM on samples of three different waste-rock types designated as 1-B, 1-C, and 1-D. Sulfide contents of these three samples are 3, 6, and 24 wt %, mainly as mixtures of euhedral and/or subhedral and framboidal pyrite (White and Jeffers 1994). The resulting experimental data from the USBM's laboratory tests are used by the University in the development of the mathematical model.

---

[1]Paper presented at the International Land Reclamation and Mine Drainage Conference and the Third International Conference on the Abatement of Acidic Drainage, Pittsburgh, PA, April 24-29, 1994.

[2]William W. White III, Geologist, U.S. Department of the Interior, Bureau of Mines, Salt Lake City Research Center, Salt Lake City, UT, USA.

[3]E. M. Trujillo, Associate Professor, and Cheng-Kuo Lin, Ph.D. Candidate, Department of Chemical and Fuels Engineering, University of Utah, Salt Lake City, UT, USA.

Proceedings America Society of Mining and Reclamation, 1993 pp 157-166
DOI: 10.21000/JASMR94010157

Several recent reviews discuss the development of AMD modeling and summarize available models (Nicholson 1992, British Columbia Acid Mine Drainage Task Force 1989). The dominant reaction for AMD production is oxidation of the common iron sulfide minerals pyrite (Stumm and Morgan 1981) and pyrrhotite (Lapakko 1980, 1988). Therefore, many of the AMD models focus on (1) oxygen as the main oxidant and (2) the various associated transport mechanisms thought to be common in waste-rock dumps. This emphasis has been successful for modeling oxidation rates and related thermal effects in site-specific applications (Davis and Ritchie 1986, Cathles and Apps 1975). However, realistic prediction of acid production (hydrogen ion concentration) and dissolution and transport of toxic metals (e.g., copper and zinc) to the receiving environment is unlikely unless oxygen-diffusion models are coupled with geochemical and hydrologic models (MEND International Workshop Proceedings 1992). A more complete AMD field model is one that couples gas transport and thermal effects with chemical kinetics and aqueous-transport mechanisms.

To facilitate understanding of AMD's complex nature, the USBM and University have chosen to first model the AMD-producing potential of discrete waste-rock types under the fixed conditions characteristic of accelerated-weathering humidity-cell tests. While conditions common to humidity-cell kinetic tests differ from those encountered in actual waste-rock dumps, reaction-controlling conditions within each cell can be fixed at predefined limits. Humidity-cell experiments (1) are essentially isothermal, (2) have an ample supply of oxygen, and (3) are characterized by well-defined gas-transport and water-flow systems. These conditions not only accelerate the weathering process but also have potential to identify rate-limiting steps characteristic of both chemical and physical processes, rather than physical processes alone (i.e., diffusion of oxygen).

The objective of the current modeling effort is to (1) predict humidity-cell effluent quality for a specific rock type and have it match experimental data for the same rock and (2) better understand the dominant geochemical mechanisms active under restricted experimental conditions.

Methods and Materials

Humidity-Cell Apparatus Description and Test Protocol

A single humidity-cell array is comprised of 16 individual cylindrical cells, each 20.3 cm long, with an inside diameter (I.D.) of 10.2 cm. Waste-rock charges for each cell are comprised of 1,000 g of sample crushed to 100% passing 1/4 in. The test protocol is comprised of weekly leach cycles that include 3 days of dry air and 3 days of wet air pumped up through the sample (at the rate of 1 L/min), followed by a drip-trickle leach with 500 mL of de-ionized water on day 7 (Lawrence 1990). Duration of the leach is approximately 2 h. Data collected weekly from each humidity cell are described in White and Jeffers (1994).

Geochemical Predictive Model

The University, under contract to the USBM, has designed a preliminary model that simulates chemical changes that occur in the weekly interstitial water remaining in each humidity cell (see White and Jeffers 1994). Rather than solve the customary diffusion and convective-transport equations for a packed column of reacting particles, a different approach has been taken. The humidity cell is conceptualized as 20 continuous-stirred tank reactor's (CSTR's) in series. Twenty CSTR's are used because this number approaches the same effluent results as a packed-bed model with axial dispersion. Currently, the model uses 10 simultaneous chemical reactions and 14 different chemical species to describe the generation and neutralization of acid in the humidity cell. Solid species include pyrite, calcium carbonate, ferric hydroxide, jarosite, and feldspar. Aqueous species include sulfate, ferrous and ferric ion, oxygen, calcium, potassium (shown as A^+ in later equations), carbonate ion, and hydrogen ion (pH). Bacterial catalysis of AMD is modeled by using a modified Monod-type relationship for the growth phase that accounts for pH dependency and includes a term that accounts for the death phase. The weekly cycle of leaching with 500 mL of de-ionized water (1 day), dry air (3 days), and then water-saturated air (3 days) is modeled, taking into account the volume change in interstitial water and the resulting evaporation.

The kinetic parameters in the model are assumed constant and dependent only on temperature, which is not a variable in these experiments. Kinetic parameters were obtained by comparing the experimental effluent compositions collected during the water-leaching phase of the weekly cycle with those predicted by the model. Input to the model includes the following parameters:

- Weight percent of total waste rock contributed by each of the major mineral constituents determined from mineral characterization
- Volume of interstitial water remaining in the humidity-cell waste-rock charge at the end of the leaching step
- Evaporation rate of interstitial water determined from the dry-air period of the weekly cycle
- Weighted-average particle size estimated from screen analysis of each sample
- Packed volume and void fraction of the humidity-cell waste-rock charge.

Once these parameters have been entered, the model calculates (1) the transient compositional changes in each CSTR with time and (2) the aqueous concentrations (including hydrogen ion as pH) predicted for the effluent sample obtained during the drip-trickle leach. The modeled effluent concentration can then be compared with experimental data.

Geochemical Reactions Included in the Model

Oxidation of Pyrite. Several mechanisms have been proposed for abiotic (Stumm and Morgan 1981, Lowson 1982) and biotic (Kleinmann et al 1981, Nordstrom 1982) oxidation. Pyrite oxidation is modeled using the four reactions listed below (equations 1-4; kinetic parameters such as KSO, KF(2), etc. listed here and in following equations are described in table 2).

$$\frac{1}{3.5}FeS_{2(s)} + O_{2(aq)} + \frac{1}{3.5}H_2O_{(l)} \xrightarrow{KSO} \frac{1}{3.5}Fe^{2+}_{(aq)} + \frac{2}{3.5}SO^{2-}_{4(aq)} + \frac{2}{3.5}H^{+}_{(aq)} \quad (1)$$

$$Fe^{2+}_{(aq)} + \frac{1}{4}O_{2(aq)} + H^{+}_{(aq)} \xrightarrow{KF(2)} Fe^{3+}_{(aq)} + \frac{1}{2}H_2O_{(l)} \quad (2)$$

$$\frac{1}{14}FeS_{2(s)} + Fe^{3+}_{(aq)} + \frac{8}{14}H_2O_{(l)} \xrightarrow{KSF} \frac{15}{14}Fe^{2+}_{(aq)} + \frac{2}{14}SO^{2-}_{4(aq)} + \frac{16}{14}H^{+}_{(aq)} \quad (3)$$

$$Fe^{2+}_{(aq)} + \frac{1}{4}O_{2(aq)} + H^{+}_{(aq)} + ?X^{?}_{(aq)} \xrightarrow{MMAX} Fe^{3+}_{(aq)} + \frac{1}{2}H_2O_{(l)} + ?X^{?}_{(aq)} \quad (4)$$

An expression for the viable bacterial population density (X) (equation 5) is derived using a modified Monod equation for the growth phase and a simple kinetic expression for the death phase. Although several rate expressions have been proposed for these types of bacteria, *Thiobacillus ferrooxidans* in particular (Shrihari 1990, Hanson 1989, Asai et al 1992, Yun and Meyerson 1982), very few account for pH effects and death rates. The growth term is a function of pH and the limiting substrate concentration, which is assumed to be the ferrous ion. The death term is a function of population density and implies that populations cannot sustain

unlimited growth because living space is limited. Additionally, the death term is implicitly related to surface area because bacteria population is also a function of ferrous ion concentration, which in turn is a function of available particle surface area. Equation 5 also provides limits to viable bacterial population densities and makes the organisms somewhat responsive to environmental conditions, although this expression is obviously not a comprehensive model. More experimental work, specifically the study of viable bacterial population densities obtained under these experimental conditions, is needed. It is also likely that a mixed culture exists in these humidity cells. If significant quantities of bacteria other than *T. ferrooxidans* are present, other expressions and reactions must be included.

$$\frac{d[X_{(aq)}]}{dt} = \mu_{max}[X_{(aq)}]\left(\frac{[H^+]}{K_{M7a} + [H^+]}\right)\left(\frac{[Fe^{2+}]}{K_{M7b} + [Fe^{2+}]}\right) - k_d[X_{(aq)}]^2 \qquad (5)$$

Neutralization. Chemical-weathering reactions not only affect metallic sulfide minerals, but also result in partial or complete dissolution of some silicate and carbonate gangue minerals comprising the bulk of the waste rock. Some of the more important gangue minerals are those that neutralize the acid being produced. Carbonates, in particular, are quite reactive and, if present in large amounts, can delay propagation of acid. Calcite and dolomite are the most common carbonate minerals, but others may also be present. The current model only considers the reaction of calcite and converts all other carbonates (except for siderite) into an equivalent amount of calcite. The reaction is given in equation 6. Calcium and carbonate are the only ions that are considered to be solubilized as a result of this neutralization reaction.

$$\frac{1}{2}CaCO_{3(s)} + H^+_{(aq)} + \frac{1}{2}H_2O_{(l)} \xrightarrow{KSCA} \frac{1}{2}Ca^{2+}_{(aq)} + \frac{1}{2}H_2CO_{3(aq)} + \frac{1}{2}H_2O_{(l)} \qquad (6)$$

For some waste-rock materials, carbonate minerals are present in trace amounts and do not contribute significantly to acid neutralization. However, once the pH reaches relatively low values, other minerals (e.g., some silicates) can begin to solubilize and react with the acid. Feldspars fall into this category and can prevent the pH from dropping to even lower values. There are many different types of feldspars with various compositions. In the present model, all feldspar-like minerals will be represented as AW; A represents the monovalent ion that is released after being solubilized (commonly potassium), and W represents the silicate component. The chemical reaction for silicate neutralization is represented by equation 7.

$$AW_{(s)} + H^+_{(aq)} \xrightarrow{KSAW} A^+_{(aq)} + HW_{(s)} \qquad (7)$$

Shrinking-Core Models. Reactions involving a solid phase are treated using the "shrinking-core" model(Fogler 1992, Levenspiel 1972). For most solid reactions, the diffusion of the reactant(s), and the counter diffusion of products through the reacted portion of the particle are rate controlling. This applies to the reactions for pyrite (equations 1 and 4), carbonate (equation 6), and feldspar (equation 7) as the radius of the shrinking core decreases appreciably. The effective diffusivities of ferric ion, dissolved oxygen, and hydrogen ion are included in the rate expressions for these solids. The amount of reactive surface area available for reaction for each of the solid species is a function of the amount of jarosite, calcium sulfate, ferric hydroxide, and ferrous carbonate that have precipitated from the interstitial water.

Precipitation. Oxidation of pyrite produces sulfate ion in solution. This ion would increase indefinitely were it not for the presence of metallic ions, particularly iron. The eventual precipitation of these sulfate salts removes metal and sulfate ions from solution, but, more importantly, produces a solid that can coat reactive pyritic surfaces. Because chemical reactions involving a solid material are a function of the reactive surface area, this coating can significantly affect the overall kinetics by providing a physical barrier between reactants. While a variety of metallic salts are possible as a result of precipitation, four species are considered significant for waste-rock samples 1-B, 1-C, and 1-D (described in White and Jeffers 1994, and shown here in table 1).

They are ferric hydroxide, jarosite, ferrous carbonate, and calcium sulfate (equations 8-11). Note that the production of ferric hydroxide is reversible, while the others are considered irreversible.

$$Fe^{3+}_{(aq)} + 3H_2O_{(l)} \xleftrightarrow[KF(-3)]{KF(3)} Fe(OH)_{3(s)} + 3H^{+}_{(aq)} \quad (8)$$

$$A^{+}_{(aq)} + 3Fe^{3+}_{(aq)} + 2SO^{2-}_{4(aq)} + 6H_2O_{(l)} \xrightarrow{KF(10)} AFe_3(SO_4)_2(OH)_{6(s)} + 6H^{+}_{(aq)} \quad (9)$$

$$Fe^{2+}_{(aq)} + CO^{2-}_{3(aq)} \xrightarrow{KF(9)} FeCO_{3(s)} \quad (10)$$

$$Ca^{2+}_{(aq)} + SO^{2-}_{(aq)} \xrightarrow{KF(5)} CaSO_{4(s)} \quad (11)$$

The precipitation of jarosite (equation 9) is affected by the solution concentrations of ferric, sulfate, and A^+ (mainly potassium) ions. As these concentrations increase, the rate of precipitation increases, forming an increasing total amount of precipitate. The jarosite precipitate presumably covers the solid materials and decreases the available surface area for the solid reactions (shrinking-core reactions), which affects the overall oxidation of pyrite.

Physical Considerations

Simulation of Humidity-Cell Weathering Cycle. The weekly cycle of the humidity-cell test has been described and is particularly challenging to model mathematically. The following assumptions have been made in order to simplify the calculations.

- During the dry-air and wet-air periods, the water in the cells is saturated with air at the appropriate temperature
- The volume of interstitial water in the humidity cell exhibits the same changes from week to week
- During the dry-air period, water is being evaporated at a constant rate
- The drip-trickle leaching step consumes 2 h each week.

The oxidation rate of pyrite, when kinetically controlled, should be a function of the liquid volume since aqueous species' concentrations are determined by the amount of water present. In some experimental settings, liquid volume is relatively constant and, thus, unimportant. However, this is not true under the conditions required for accelerated-weathering tests using humidity cells. Interstitial water volume in the waste-rock charge changes throughout the week owing to air drying and resaturation with de-ionized water. Consequently, concentrations of the various aqueous species contained in the interstitial water vary considerably over the weekly cycle. This is taken into consideration by adjusting concentrations within the cell based on the amount of interstitial water. The critical volumes are those after the drying cycle and those associated with the leaching step and subsequent elution.

Oxygen Diffusion. Because air is pumped continuously through each humidity cell at 1.0 L/min for both the wet- and dry-air cycles, the concentration of oxygen in the interstitial water is assumed to be constant at saturated conditions during this time period. During the leaching step, however, air is not being pumped and oxygen in the aqueous phase is allowed to decrease in accordance with its consumption for the designated

chemical reactions. As stated earlier, the solid reactions include the effects of oxygen diffusion through the reacted portion of the particles.

Particle Size Versus Reactive Surface Area. Most cells have a rather broad distribution of particle sizes depending on how the sample is taken and if only a certain size fraction is used. The description of the particles within the cell has been simplified by using a weighted average particle size for each rock type based on experimentally-determined weight and size distributions.

Numerical Techniques

One-dimensional, unsteady-state material balances are calculated for each species in each CSTR. The 280 simultaneous differential equations (20 CSTR's times the number of species, which is 14 at this point) were solved for each time increment using the Runge-Kutta fourth-order method coded in FORTRAN. The model predicts the effluent concentrations for the aqueous species from the last CSTR as a function of time during the drip-trickle leach step. These point concentrations are then integrated over the appropriate time period to give an average concentration in the collected effluent for each species, which can then be compared with experimental data.

Results and Discussion

Geochemical Predictive Model

Input Parameters. The most critical input to the model is the suite of dominant mineral species contained in each waste-rock type that comprises the bulk of the waste dump. The major mineral species comprising samples 1-B, 1-C, and 1-D are contained in table 1; weight-percent estimates for these minerals were determined by image analysis and are also summarized.

Table 1. Weight-percent estimates of major mineral constituents in waste-rock samples 1-B, 1-C, and 1-D.

Mine sample	Rock type	Major mineral constituents (est. wt %)						
		Qtz[1]	K-spar[2]	Plag[3]	Clay	$CaCO_3$[4]	Pyrite	Po[5]
1-B ..	Latite porphyry ...	30	26	22	2	0	6	ND
1-C ..	Massive-sulfide mudstone	30	12	8	5	.2	24	ND
1-D ..	Mudstone	40	18	20	2	.3	3	Tr

ND Not detected.
Tr Trace.
[1]Quartz.
[2]Potassic feldspar.
[3]Plagioclase.
[4]White and Jeffers (1994), table II.
[5]Pyrrhotite.

Although all three samples are from the same mine, minerals common to each vary markedly in abundance (especially pyrite). While carbonate is present in two of the three samples, its presence is minimal compared with the amount of pyrite contained in all three samples. A more detailed presentation and discussion of the mineral-characterization results for each of the three samples is contained in White and Jeffers (1994).

Another important model input is the average particle-size diameter for each sample. Average particle-size diameters for samples 1-B, 1-C, and 1-D are 1.3, 2.9, and 3.4 mm, respectively.

Kinetic Parameters. Fifteen kinetic parameters have been derived for the current model and are shown in table 2.

Table 2. Kinetic parameters used in geochemical model

Parameter	Description	Model value	Literature value(s)	Reference(s)
KF(2)	Abiotic oxidation of ferrous ion.	1.0×10^{-7} mmol/L/h	NAp	
KF(3)	Formation of ferric hydroxide.	4.0×10^{-7} mmol/L/h	NAp	
KE(3)	Equilibrium constant for ferric hydroxide.	2.0×10^{-3} $(mmol/L)^{-2}$	NAp	Stumm (1981)
KF(5)	Precipitation of calcium sulfate.	1.0×10^{-5} mmol/L/h	NAp	
KF(9)	Precipitation of ferrous carbonate.	1.0×10^{-3} mmol/L/h	NAp	
KF(10)[1]	Precipitation of jarosite.	4.07×10^{-15} mmol/L/h	NAp	
K_{M7a}	Monod-type constant for hydrogen ion in bacteria growth equation.	0.1 mmol/L	NAp	
K_{M7b}	Monod-type constant for ferrous ion in bacteria growth equation.	2.0 mmol/L	2.2 mmol/L 2.5 mmol/L 2.55 mmol/L 2.2 to 5.4 mmol/L	Ehrlich (1990) Yun (1982) Myerson (1984) Schnaitman (1969)
μ_{MAX}	Maximum growth rate.	0.1/h	0.183/h 0.05 to 0.25/h 0.104/h 0.1085/h	Shrihari (1990) Hanson (1989) Asai (1992) Yun (1982)
K_d	Bacteria death-phase constant.	5.0×10^{-2} mmol/L/h	NAp	
$Y_{X/Fe}$	Yield coefficient.	0.4 mg bacteria/ (mmol Fe^{+2})	0.09 to 0.5 mg bacteria/ (mmol Fe^{+2})	Hanson (1989)
KSO	Direct oxidation of pyrite by dissolved oxygen.	1.5×10^{-11} $L/cm^2/sec$	NAp	
KSF	Oxidation of pyrite by ferric ion.	5.0×10^{-11} $L/cm^2/sec$	NAp	
KSCA[2]	Reaction of calcium carbonate with acid.	1.0×10^{-7} $L/cm^2/sec$	8.65×10^{-6} $L/cm^2/s$ for pure calcite	Busenberg (1986)
KSAW	Reaction of feldspars with acid.	8.0×10^{-12} $L/cm^2/sec$	2.28×10^{-13} $L/cm^2/s$ for pure albite	Blum (1988)

NAp Not applicable.
[1]For sample 1-B, a value of 2.33×10^{-10} was used.
[2]For samples 1-B and 1-C, a value of 2.0×10^{-12} was used.

The magnitude of each kinetic parameter was initially established by applying trial and error curve-fitting techniques to the experimental data. Sensitivity analysis was then performed to assess the importance of each kinetic parameter on the modeled output. The resulting calculated parameters have been compared with corresponding kinetic parameters available in the literature and demonstrate reasonable agreement. Note that all but two of the kinetic-parameter values are the same for each of the three samples. The two exceptions are for the precipitation of jarosite and the dissolution of calcium carbonate (constants KF(10) and KSCA, respectively).

The value of the jarosite precipitation rate constant for sample 1-B was changed from 4.07×10^{-15} (used for 1-C and 1-D) to 2.33×10^{-10}. Rationale for this change is the possibility that other species are being precipitated in sample 1-B, but not in the other two samples.

The rate constant for the reaction of calcium carbonate with acid was changed from 1.0×10^{-7} to 2.0×10^{-12} for samples 1-B and 1-C. This change is more difficult to justify. Carbonate content in each of the three samples was too low to identify discrete mineral composition by X-ray diffraction (XRD) analysis. Because sample 1-D contained the only visually-observed carbonate (White and Jeffers 1994), it has been assigned a value closer to the calcite rate constant until further characterization can be completed, and more published carbonate-rate constants can be found.

Correlation of Modeled Output With Experimental Data. Preliminary fit of model-generated data to corresponding experimental data from 90 weeks of humidity-cell testing is encouraging. Figures 1 through 3 compare model-predicted pH, total iron, and sulfate concentrations with corresponding weekly effluent

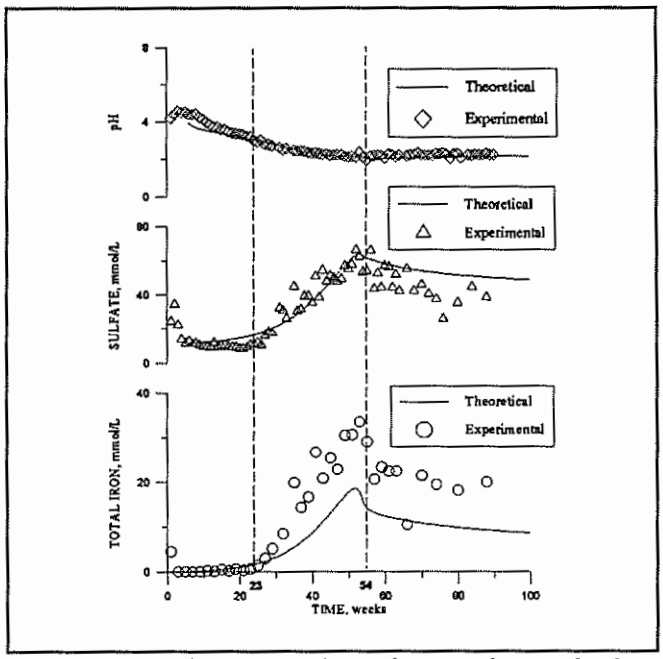

Figure 1. Ninety weeks of experimental data obtained from sample 1-C compared with modeled output.

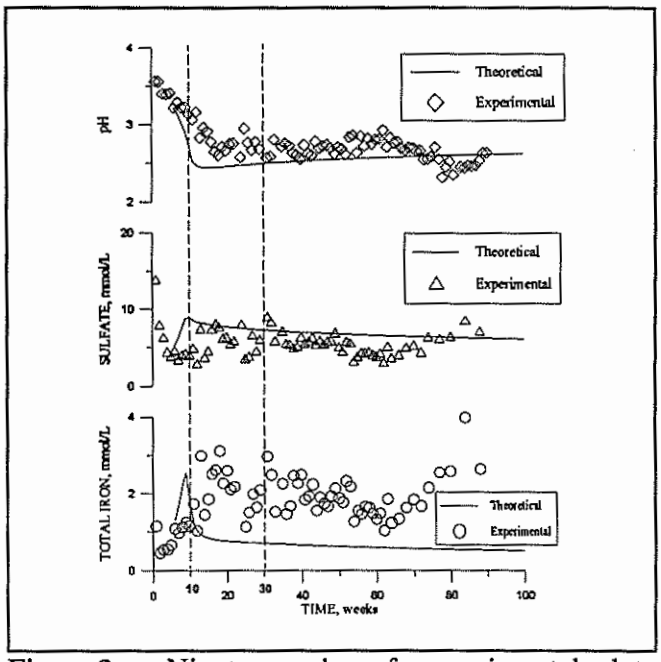

Figure 2. Ninety weeks of experimental data obtained from sample 1-B compared with modeled output.

concentrations from samples 1-B, 1-C, and 1-D.

The model duplicated two critical experimental responses, which are illustrated by sample 1-C in figure 1. The first is transition of the pyrite-oxidation mechanism from abiotic (oxygen only) to biotic (bacteria catalyzed) oxidation at pH 3. The second is the effect of jarosite precipitation on pH, sulfate, and total-iron concentrations at week 54. Elapsed time required for weekly effluent to reach a pH of 3 was 23 weeks. A correlative increase in sulfate and total iron concentrations also occurred at week 23. These concentrations continued to increase until week 54, when they started to decrease. By week 54, a yellow precipitate was visible in sample 1-C, and later identified as jarosite by XRD. Total iron and sulfate concentrations continued to decrease from week 54 to week 90. This decrease in concentration is from the coating of exposed pyrite surfaces by jarosite precipitate and consequent reduction in the pyrite-oxidation rate.

Output from the model is generally in good agreement with these experimental data from sample 1-C, and in fair agreement with samples 1-B and 1-D. This is encouraging considering that with two exceptions, all the kinetic rates have been held constant for all three samples. Modeled output for sample 1-B

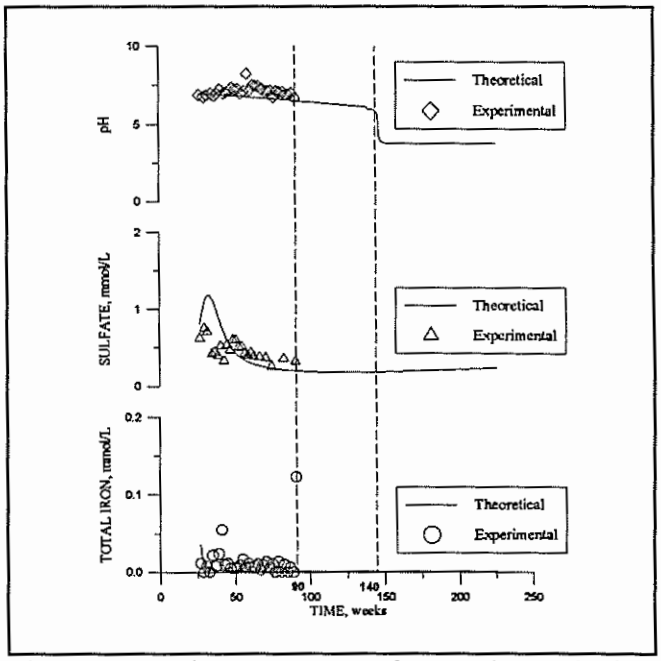

Figure 3. Ninety weeks of experimental data obtained from sample 1-D compared with modeled output.

predicted that pH would drop below 3 near weeks 8 to 10 with concurrent increases in total iron and sulfate concentrations; effects of jarosite precipitation (i.e., concurrent reduction in total iron and sulfate concentrations) would start within the same time frame. Experimental data from sample 1-B effluent closely matched modeled output for pH, but demonstrated a significant lag time between modeled effects of jarosite precipitation and actual effects at 30 weeks. For sample 1-D, the model predicts that effluent pH will decrease very slightly, but remain in the neutral range until after week 130, when it drops precipitously from pH 6 to 4. Although current experimental data are only available for 90 weeks of testing, existing pH data from weekly effluent closely match model-predicted values. White and Jeffers (1994) predicted a similar drop in effluent pH during the period 110 to 130 weeks based on experimental calcium plus magnesium release rates from 51 weeks of humidity-cell testing. Because these rates have not changed appreciably from 51 to 90 weeks, the estimate is still expected to match modeled predictions for sample 1-D effluent.

Summary and Conclusions

Preliminary fit of model-generated data to 90 weeks of humidity-cell accelerated-weathering test data is promising for three different waste-rock samples. The current version of the model has duplicated two critical experimental responses observed in the humidity-cell testing. The first is the transition from abiotic to biotic pyrite oxidation. The second reflects the precipitation of jarosite and the concurrent reduction of total iron and sulfate concentrations due to precipitate coating of rock particles and consequent reduction in the pyrite-oxidation rate. Modeled output is in good agreement with experimental data for one waste-rock sample and exhibits reasonable agreement with two additional waste-rock samples. With two exceptions, these matches have been achieved without manipulating the 15 calculated rate constants for respective reactions that govern the operation of the current model. To enhance the model's application to a broader range of waste-rock types, additional solid- and liquid-phase species will be added to the model as new waste-rock types are characterized. Examples include the minerals chalcopyrite and pyrrhotite, elemental sulfur, and aqueous species of copper and zinc.

Literature Cited

Asai, S., Y. Konishi, and K. Yoshida. 1992. Kinetic model for bacterial dissolution of pyrite particles by *Thiobacillus ferrooxidans*. Chemical Eng. Sci. 47(1):133-139. http://dx.doi.org/10.1016/0009-2509(92)80207-S

Blum, A. and A. Lasaga. 1988. Role of surface speciation in the low-temperature dissolution of minerals. Nature 331:431-433. http://dx.doi.org/10.1038/331431a0

British Columbia Acid Mine Drainage Task Force. 1989. Draft acid rock drainage technical guide. Can. Dept. Energy, Mines, and Resources, Vancouver, BC, Canada, v. 1, 260 pp.

Busenberg, E. and L. N. Plummer. 1986. A comparative study of the dissolution and crystal growth kinetics of calcite and aragonite. U.S. Geol. Surv. Bull. 1578.

Cathles, L. M. and J. A. Apps. 1975. Model of the dump leaching process that incorporates oxygen balance, heat balance, and air convection. Metall. Trans. B 6B:617-624. http://dx.doi.org/10.1007/BF02913857

Davis, G. B. and A. I. M. Ritchie. 1986. A model of oxidation in pyritic mines wastes: Part 1, Equations and approximate solution. Appl. Math. Modelling 10:314-322. http://dx.doi.org/10.1016/0307-904X(86)90090-9

Ehrlich, H. L. 1990. Geomicrobiology, 2d ed. Marcel Dekker, Inc. Ch 14.

Fogler, H. S. 1992. Elements of chemical reaction engineering, 2d ed. Prentice Hall International, NJ. p. 582-589.

Hanson, J. S. 1989. Kinetic model of the bacteria leaching of chalcopyrite concentrates. Dep. Mat. Sci. and Min. Eng. Univ. of CA-Berkeley.

Kleinmann, R. L. P., D. A. Crerar, and R. R. Pacelli. 1981. Biogeochemistry of acid mine drainage and a method to control acid formation. Min. Eng. 33:300-305.

Lapakko, K. A. 1980. Kinetics and mechanisms of the oxidative dissolution of metal sulfide and silicate minerals present in the Duluth Gabbro. M.S. Thesis. Univ. of MN, Minneapolis, MN. 199 p.

Lapakko, K. A. 1988. Prediction of acid mine drainage from Duluth Complex mining wastes in northeastern Minnesota. p. 180-190. In Proceedings of 1988 Mine Drainage and Surface Mine Reclamation Conference, v.1. BuMines IC 9183.

https://doi.org/10.21000/JASMR88010180

Lawrence, R. W. 1990. Prediction of the behaviour of mining and processing wastes in the environment. p. 115-121. In Proceedings of the Western Regional Symposium on Mining and Mineral Processing Wastes. (Berkeley, CA, May 30-June 1, 1990).

Levenspiel, O. 1972. Chemical reaction engineering, 2d ed. Wiley, New York. p. 361-374.

Lowson, R. T. 1982. Aqueous oxidation of pyrite by molecular oxygen. Chem.Reviews 82(5):461-497. http://dx.doi.org/10.1021/cr00051a001

Mine Environment Neutral Drainage (MEND) Program. 1992. 52 p. In Proceedings of the International Workshop on Waste Rock Modelling. (Toronto, ON, September 29-October 1, 1992).

Myerson, A. S. and P. C. Kline. 1984. Continuous bacterial coal desulfurization employing *Thiobacillus ferrooxidans*. Biotechnol. and Bioeng. 26:92-99.
http://dx.doi.org/10.1002/bit.260260117

Nicholson, R. V. 1992. A review of models to predict acid generation rates in sulphide waste rock at mine sites. p. 41-52. In Proceedings of the International Workshop on Waste Rock Modelling. (Toronto, ON, September 29-October 1, 1992).

Nordstrom, D. K. 1982. Aqueous pyrite oxidation and the consequent formation of secondary iron minerals. p. 37-56. In Acid sulfate weathering. J. A. Kittrick, D. S. Fanning, and L. R. Hossner (eds.), Soil Sci. Soc. America Spec. Pub. 10.

Schnaitman, C. A. , M. S. Korczynski, and D. G. Lundgren. 1969. Kinetic studies of iron oxidation by whole cells of *Thiobacillus ferrooxidans*. J. Bacteriology 99:552-557.

Shrihari, R. K. and K. S. Gandhi. 1990. Modelling of Fe2+ oxidation by *Thiobacillus ferrooxidans*. Appl. Microbiol.and Biotechnol. 33:524-528.

Stumm, W. and J. J. Morgan. 1981. Aquatic Chemistry. Wiley-Interscience, New York. p. 241, 469-471.

White, W. W. and T. H. Jeffers. 1994. Chemical predictive modelling of acid mine drainage from metallic sulfide-bearing waste rock. p. 608-630. In Proceedings of American Chemical Society Symposium Series 550.

Yun, C. C. and A. S. Myerson. 1982. Growth models of the continuous bacterial leaching of iron pyrite by *Thiobacillus ferrooxidans*. Biotechnol. and Bioeng. 24:889-902.
http://dx.doi.org/10.1002/bit.260240411